JOURNAL OF AIRCRAFT
Vol. 44, No. 2, March–April 2007

# Nonlinear Aeroelastic Analysis for a Control Fin with an Actuator

Won-Ho Shin* and In Lee†
*Korea Advanced Institute of Science and Technology, Daejeon 305-701, Republic of Korea*
Young-Sug Shin‡
*Agency for Defense Development, Daejeon 305-701, Republic of Korea*
and
Jae-Sung Bae§
*Hankuk Aviation University, Seoul 200-1, Republic of Korea*

DOI: 10.2514/1.24721

**Nonlinear aeroelastic characteristics of a control fin with an actuator were investigated, including the structural nonlinearity, by using the iterative v-g method. System identification of an actuator was performed with a sine sweep test, and the doublet-hybrid method was used to calculate unsteady aerodynamic forces. Structural nonlinearity located in the load links of the actuator was considered and assumed to be the freeplay. Nonlinear aeroelastic analyses were performed in both the frequency and time domains, and the nonlinear flutter analyses showed that the flutter characteristics significantly depend on the structural nonlinearity as well as the effects of the actuator. The results also indicate that it is necessary to consider seriously the effects of the poles and zeros of the actuator on the flutter characteristics to predict flutter behavior accurately when designing the actuators of missiles or aircraft.**

## Nomenclature

| | | |
|---|---|---|
| $bl$ | = | size of freeplay |
| $\tilde{\mathbf{C}}$ | = | generalized damping matrix |
| $C_L$ | = | damping of load links |
| $C_m$ | = | damping of electric motor |
| $c_1$ | = | damping of first gear |
| $f_{\text{flutter}}$ | = | linear flutter frequency |
| $J_L$ | = | moment of inertia of load links |
| $J_m$ | = | moment of inertia of electric motor |
| $J_1$ | = | moment of inertia of first gear |
| $J_2$ | = | moment of inertia of second gear |
| $\mathbf{K}$ | = | generalized stiffness matrix |
| $K_L$ | = | static stiffness of load links |
| $K_m$ | = | static stiffness of electric motor |
| $K_\theta$ | = | linear static root stiffness |
| $k$ | = | stiffness between second gear and load links |
| $k_1$ | = | stiffness of first gear |
| $\mathbf{M}$ | = | generalized mass matrix |
| $N_1$ | = | first gear reduction |
| $N_2$ | = | second gear reduction |
| $T$ | = | torque induced by electric motor |
| $T_1$ | = | transmission torque from motor to first gear |
| $T_L$ | = | transmission torque from second gear to load links |
| $U_{\text{flutter}}$ | = | linear flutter velocity |
| $\beta$ | = | transmission error |
| $\delta$ | = | nondimensional displacement |
| $\theta_L$ | = | rotational displacement of load links |
| $\theta_m$ | = | rotational displacement of electric motor |
| $\theta_n$ | = | rotational displacement of second gear |
| $\theta_1$ | = | rotational displacement of fist gear |
| $\Phi_F$ | = | modal matrix |

Received 20 April 2006; accepted for publication 20 October 2006. 

*Graduate Research Assistant, Division of Aerospace Engineering, Department of Mechanical Engineering, 373-1 Guseong-Dong, Yuseong-Gu; swh@asdl.kaist.ac.kr.

†Professor, Division of Aerospace Engineering, Department of Mechanical Engineering, 373-1 Guseong-Dong, Yuseong-Gu; inlee@asdl.kaist.ac.kr. Associate Fellow AIAA (corresponding author).

‡Principal Researcher, PO Box 35-3, Yuseong-Gu; sys5987@yahoo.co.kr.

§Assistant Professor, School of Aerospace and Mechanical Engineering; jsbae@hau.ac.kr. Member AIAA.

## I. Introduction

CONSIDERATION of static and dynamic aeroelasticity presents important challenges in aircraft and missile design. Flutter is an aeroelastic instability, whereas aeroelasticity is the discipline that studies the interaction among elastic, aerodynamic, and inertia forces. Such aeroelastic phenomena cause the failure of flight vehicle structures or the decline of control performances. Therefore, it is necessary to predict aeroelastic characteristics accurately to avoid aeroelastic instabilities. Recently, the actuators get precise and minute; in addition, the control systems of wings become complex for good flight performance. Thus the number of researchers studying controllers is steadily growing. As actuators become more advanced, the effects of actuator dynamics on wing aeroelasticity have become more significant.

Aeroelastic analyses of flight vehicles are easily performed under an assumption of structural and aerodynamic linearity. The analytical aeroelastic results using this assumption, however, may differ considerably from real phenomena, because most actual structures may include structural nonlinearities, such as freeplay and backlash, which occur during the manufacturing process. Previous studies showed that nonlinear aeroelastic characteristics sometimes differed significantly from linear ones [1,2] and aeroelastic behaviors with an actuator dynamics were considerably different from those of wing only [3]. Linear aeroelastic responses typically include flutter and divergence, but nonlinear aeroelastic responses also include limit-cycle oscillation (LCO) and chaotic motion. LCO is a periodic oscillation that consists of a limited number of periods, while chaotic motion is a nonperiodic oscillation.

The amplitude of the aeroelastic response increases exponentially when a linear system becomes unstable. In contrast, a nonlinear system often has a bounded motion, such as LCO or a chaotic motion below or above the linear flutter speed. The LCO and chaotic motion do not cause the abrupt failure of structures. However, these motions can cause a structure to be damaged by fatigue and can considerably affect the control systems of flight vehicles. Thus, the effects of both

structural nonlinearities and actuator dynamics on the aeroelastic characteristics of flight vehicles should be considered during the design stage.

Several investigators have performed nonlinear aeroelastic analyses of flight vehicles with structural nonlinearities or actuator dynamics. Woolston et al. [1] analyzed a nonlinear aeroelastic system with freeplay, hysteresis, and cubic nonlinearity, and they showed that LCO may occur below the linear flutter boundary. Laurenson and Tron [2] studied the flutter of a missile control surface with freeplay at the hinge direction using the describing function method. Yehelzkely and Karpel [3] presented a method for flutter analysis and design of missiles having pneumatic missile fin actuators, and they showed that the fundamental fin flutter speed is strongly dependent on the missile maneuver commands. McIntosh et al. [4] performed experimental and theoretical studies of nonlinear flutter for a typical section model with hardening or softening spring in hinge and plunge directions, and they observed limit-cycle and divergent amplitude-sensitive instabilities. Yang and Zhao [5] studied the LCO of a typical section model with nonlinearity in the pitch direction subject to incompressible flow using the Theodorsen function. Lee and Tron [6] carried out a flutter sensitivity study for a CF-18 aircraft with a wing-folding hinge and investigated the flutter characteristics and effects on a limit-cycle flutter at the wing fold of aileron angles.

Lee and Kim [7] studied the LCO and chaotic motion of a missile control surface with freeplay using a time-domain analysis. Paek and Lee [8] performed a flutter analysis for a control surface of a launch vehicle with control actuators and investigated the effect of the sweep angle on the flutter characteristics of the wing with dynamic stiffness. Conner et al. [9] performed numerical and experimental studies on the nonlinear aeroelastic characteristics of a typical section with control surface freeplay. Liu and Chan [10] investigated the limit-cycle oscillation phenomenon for a nonlinear aeroelastic system under unsteady aerodynamics, and they showed that wind tunnel test results agreed well with predictions obtained both theoretically and numerically. Paek et al. [11] studied the flutter characteristics of a wraparound fin while considering rolling motion and aerodynamic nonlinearity. Librescu et al. [12] dealt with a study of the benign and catastrophic characters of the flutter instability boundary of 2-D lifting surfaces in a supersonic flowfield, and they studied the bifurcational behavior of an aeroelastic system near a flutter boundary using a method based on the first Lyapunov quantity. Bae et al. [13] investigated the nonlinear aeroelastic characteristics of a deployable missile control fin, and they observed three different types of limit-cycle oscillations over a wide range of airspeeds beyond the linear flutter boundary. Although many studies have been performed for nonlinear flutter, the nonlinear flutter analyses that consider both structural nonlinearity and the dynamic effect of control systems have not yet been performed.

In the present study, the nonlinear aeroelastic characteristics of a missile fin with an actuator (shown in Fig. 1) are investigated with consideration of structural nonlinearity as well as the dynamics of an actuator. The nonlinearity of the fin-actuator joints is represented by freeplay, and the transfer function of the actuator is obtained via a rational function comprised system of coefficients from dynamic tests. The finite element method is used for the free vibration analysis, and the doublet-hybrid method (DHM) [14] is used for the computation of unsteady aerodynamic forces, which are approximated using Karpel's method [15]. The fictitious mass (FM) method [16] is used to reduce the problem size and the computation time.

## II. Theoretical Analysis

### A. Governing Equation of Actuator

Figure 2 indicates the free-body diagram of an actuator, and the governing equation of the actuator, which consists of an electric motor, gears, and load links, can be obtained using Newton's method at each point. The governing equation of a motor can be written as combination mass, damping, and stiffness of a motor at point A:

$$J_m\ddot{\theta}_m + C_m\dot{\theta}_m + K_m\theta_m = T - T_1 \tag{1}$$

The equation of motion of gear 1 at point B can be represented as

$$\frac{1}{N_1}\{J_1\ddot{\theta}_1 + c_1(\dot{\theta}_1 - \dot{\theta}_n) + k_1(\theta_1 - \theta_n)\} = T_1 \tag{2}$$

where

$$\theta_m = N_1\theta_1 \tag{3}$$

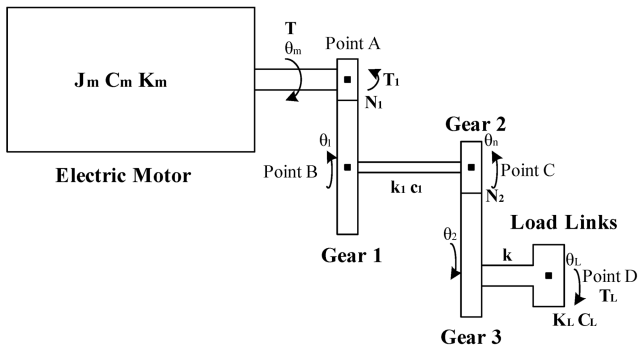


a) The free-body diagram of gear systems

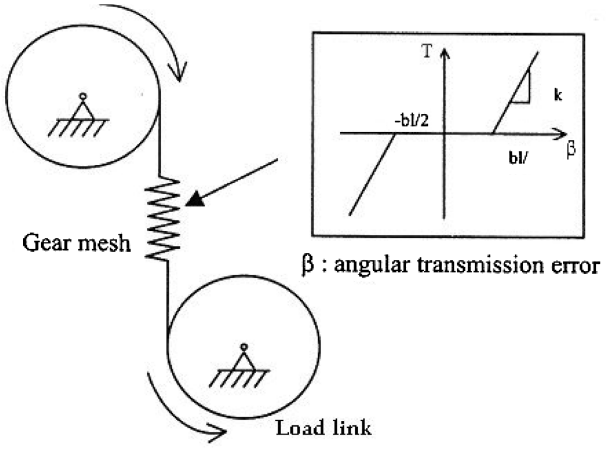


b) Backlash model of the gear system

Fig. 2 The free-body diagram and backlash model of the gear system.

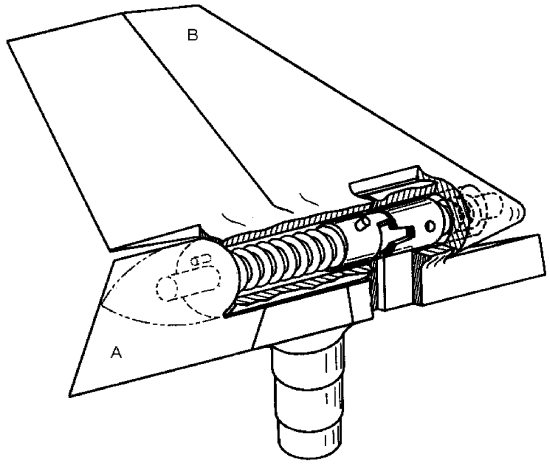


Fig. 1 The geometry of the missile fin.

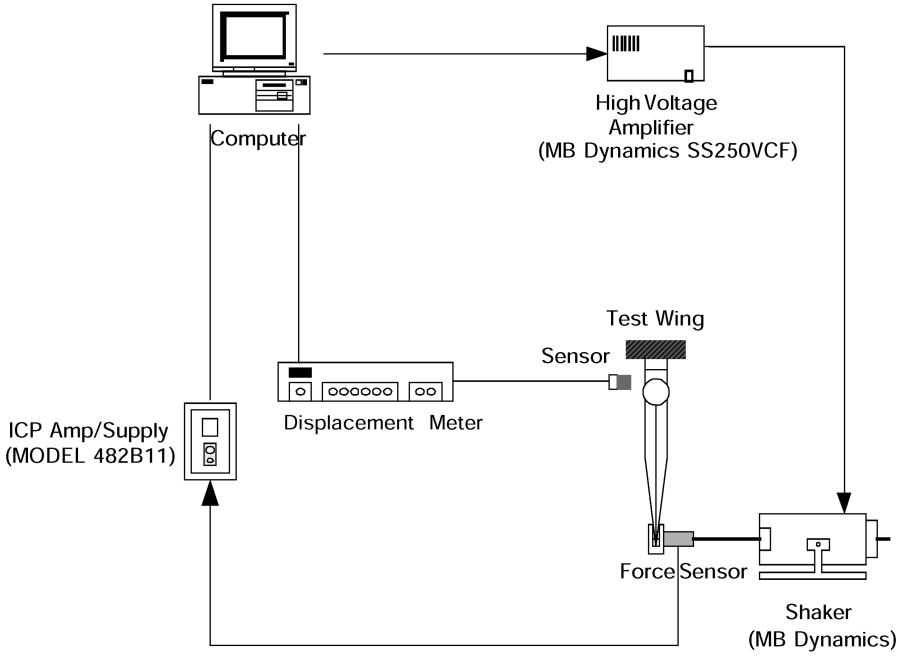


**Fig. 3 Experimental setups for measuring displacement response of the missile fin system.**

Applying Eq. (3) to Eq. (2), Eq. (2) can be changed into

$$J_1 \frac{\ddot{\theta}_m}{N_1} = N_1 T_1 - c_1\left(\frac{\dot{\theta}_m}{N_1} - \dot{\theta}_n\right) - k_1\left(\frac{\theta_m}{N_1} - \theta_n\right) \tag{4}$$

The equation of motion at point C can be obtained as Eq. (5), and Eq. (5) can be represented as Eq. (6):

$$J_2\ddot{\theta}_n + c_1\left(\dot{\theta}_n - \frac{\dot{\theta}_m}{N_1}\right) + k_1\left(\theta_n - \frac{\theta_m}{N_1}\right) = -\frac{T_L}{N_2} \tag{5}$$

$$J_2\ddot{\theta}_n = -c_1\left(\dot{\theta}_n - \frac{\dot{\theta}_m}{N_1}\right) - k_1\left(\theta_n - \frac{\theta_m}{N_1}\right) - \frac{T_L}{N_2} \tag{6}$$

There is a transmission error between gear 3 and the load axis. Transmission error $\beta$ can be written as follows:

$$\beta = \theta_1 - \theta_L = \frac{\theta_n}{N_2} - \theta_L \tag{7}$$

The transmission torque can be represented with the multiple between stiffness and transmission error:

$$T_L = k\beta \tag{8}$$

The equation of motion at point D can be obtained as

$$J_L\ddot{\theta}_L + C_L\dot{\theta}_L + K_L\theta_L = T_L \tag{9}$$

**Table 1 Information of the experimental test of the missile system**

| No. | Sine sweep range | Force |
|---|---|---|
| Test 1 | 5–500 Hz | 23 kgf |
| Test 2 | 5–500 Hz | 14 kgf |
| Test 3 | 5–250 Hz | 23 kgf |
| Test 4 | 5–500 Hz | 42 kgf |
| Test 5 | 5–250 Hz | 42 kgf |

Assuming that the moments of inertia of gears are negligibly small and solving Eqs. (1–9), the transfer function of the actuator can be represented as

$$\frac{T(s)}{\theta_L(s)} = N_1(J_m s^2 + C_m s + K_m)\left[\left\{\frac{1}{N_2(k_1 + c_1 s)} + \frac{1}{k}\right\} \times (J_L s^2 + C_L s + K_L) + N_2\right] + \frac{J_L s^2 + C_L s + K_L}{N_1 N_2} \tag{10}$$

Structural nonlinearities, including backlash, freeplay, or transmission error, can be present in the actuator throughout the experimental test, and structural nonlinearity of the actuator is assumed to be the freeplay of the load links. Relations (as shown in Fig. 2b) between the nonlinear restoring force and the displacement can be written as

$$f(\beta) = \begin{cases} 0 & \text{for } |\beta| < bl \\ k(\beta - bl) & \text{for } |\beta| > bl \end{cases} \tag{11}$$

The equivalent stiffness of a nonlinear spring in Eq. (11) should be obtained for performing the nonlinear flutter analysis in the frequency domain. The general describing function method [17] can give the stiffness of an equivalent linear system. The principal advantage of the describing function method is that it serves as a valuable aid to the design of a nonlinear system, using the Furie series expansion subject to bias, sinusoidal, or random inputs. The describing function of Eq. (11) can be written as

$$\psi(\beta) = 1 - \frac{2}{\pi}\left[\sin^{-1}\frac{bl}{\beta} + \frac{bl}{\beta}\sqrt{1 - \left(\frac{bl}{\beta}\right)^2}\right] \tag{12}$$

### B. Aeroelastic Equations

The aeroelastic equations of the missile fin with concentrated structural nonlinearity can be written as

$$\mathbf{M}\ddot{\mathbf{u}} + \mathbf{C}\dot{\mathbf{u}} + \mathbf{K}_u(\omega, \mathbf{u})\mathbf{u} = \mathbf{F}(t, \mathbf{u}, \dot{\mathbf{u}}) \tag{13}$$

where $\mathbf{M}$, $\mathbf{C}$, and $\mathbf{u}$ are a mass matrix, a damping matrix, and displacement, respectively. In addition, $\mathbf{F}(t, \mathbf{u}, \dot{\mathbf{u}})$ is the unsteady aerodynamic force and $\mathbf{K}_u(\omega, \mathbf{u})$ is the nonlinear stiffness matrix.

The nonlinear stiffness matrix is divided into linear and nonlinear terms, which can be written as

$$\mathbf{K}(\omega, \mathbf{u})\mathbf{u} = \mathbf{K}(\omega)\mathbf{u} + f(\omega, \mathbf{u})u \tag{14}$$

where $\mathbf{K}(\omega)$ is a frequency-dependent stiffness matrix, and $f(\omega, \mathbf{u})$ is the restoring force vector. The modal coordinates are used to reduce the system size and computational time in the aeroelastic analysis. Because the nonlinear stiffness matrix and mode shapes vary with the behavior of the system in an aeroelastic system with structural nonlinearity and dynamic stiffness, the aeroelastic results may be inaccurate in the constant modal coordinate of the nominal model. However, it takes too much time to redefine the modal coordinates of the aeroelastic system for accurate results as the nonlinear stiffness matrix and mode shapes vary. The advantage of the FM method is that it can consider the changes of stiffness in modal coordinates without redefining the modal coordinates.

The fictitious mass method, suggested by Karpel [18], is used to couple several substructures. The fictitious mass is added to interface coordinates of substructure. The equation of motion adding fictitious mass $\mathbf{M_F}$ is rewritten as

$$(\mathbf{M} + \mathbf{M_F})\ddot{\mathbf{u}} + \mathbf{C}\dot{\mathbf{u}} + \mathbf{K}\mathbf{u} = \mathbf{F}(t, \mathbf{u}, \dot{\mathbf{u}}) \tag{15}$$

The eigenvector and eigenvalue matrices are obtained solving the eigenvalue problem of Eq. (15). When the modal matrix $\mathbf{\Phi_F}$ of the FM model is used, the structural displacement vector can be transformed into modal coordinates as follows:

$$\mathbf{u} = \mathbf{\Phi_F}\boldsymbol{\eta} \tag{16}$$

where $\boldsymbol{\eta}$ is the displacement vector in modal coordinates. Then, the generalized aerodynamic forces can be written as

$$\bar{\mathbf{F}} = \mathbf{\Phi_F}\mathbf{F} = \mathbf{q}\mathbf{\Phi}_\mathbf{F}^\mathbf{T}\mathbf{Q}\mathbf{\Phi_F}\boldsymbol{\eta} = \mathbf{q}\bar{\mathbf{Q}}\boldsymbol{\eta} \tag{17}$$

where $\mathbf{q}$ and $\bar{\mathbf{Q}}$ are the dynamic pressure and the generalized aeroelastic coefficient matrix, respectively. The governing equation of the real structure differing $\mathbf{\Delta K}$ with the previous structure is written as

$$\mathbf{M}\ddot{\mathbf{u}} + \mathbf{C}\dot{\mathbf{u}} + (\mathbf{K} + \Delta\mathbf{K})\mathbf{u} = \mathbf{F}(t, \mathbf{u}, \dot{\mathbf{u}}) \tag{18}$$

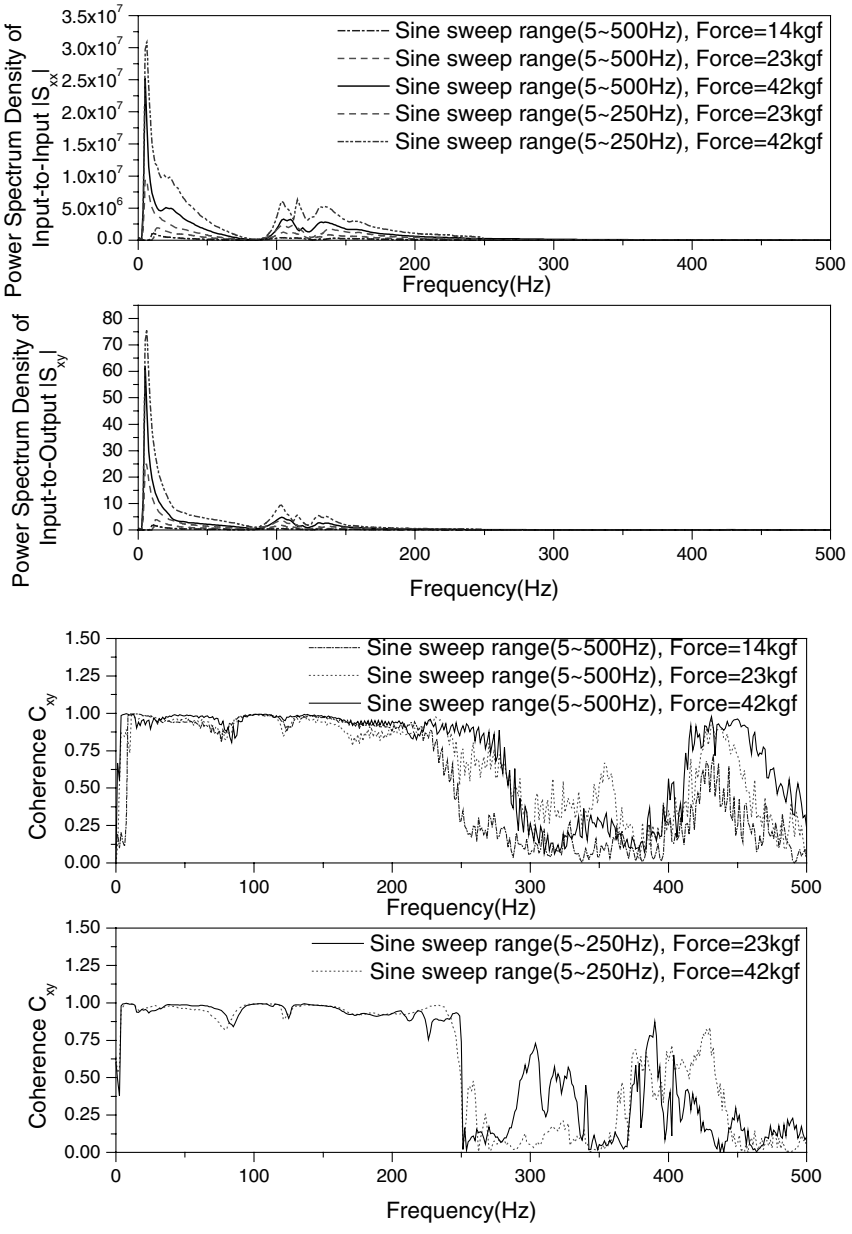


**Fig. 4 Power spectrum densities of experimental tests of the missile fin system.**

Equation (18) can be rewritten as

$$(\bar{\mathbf{M}} - \boldsymbol{\Phi}_{\mathbf{F}}^{\mathrm{T}}\mathbf{M}_{\mathbf{F}}\boldsymbol{\Phi}_{\mathbf{F}})\ddot{\boldsymbol{\eta}} + \bar{\mathbf{C}}\,\dot{\boldsymbol{\eta}} + [\bar{\mathbf{K}}(\omega) + \boldsymbol{\Phi}_{\mathbf{F}}^{\mathrm{T}}\boldsymbol{\Delta}\mathbf{K}\boldsymbol{\Phi}_{\mathbf{F}}]\boldsymbol{\eta} = \mathbf{q}\bar{\mathbf{Q}}\boldsymbol{\eta} - \boldsymbol{\Phi}_{\mathbf{F}}^{\mathrm{T}} f(\omega, \mathbf{u}) \tag{19}$$

Although $\boldsymbol{\Delta}\mathbf{K}$ has various values, $\boldsymbol{\Phi}_{\mathbf{F}}$ is consistently used to construct the generalized coordinate. It does not need to calculate the aerodynamics and to perform the free vibration analysis again when the changes of the structure occur. The fictitious mass method is the efficient and simple method to perform the aeroelastic analysis for the nonlinear structure.

Karpel's minimum-state rational-function approximations of unsteady aerodynamic force coefficient matrices for time-domain state-space aeroelastic analysis are used, obtaining the iterative nonlinear least-square solution. The aeroelastic response in the time domain can be obtained, integrating the state-state equation of Eq. (17). The approximation form of Karpel's method is represented as

$$\bar{\mathbf{Q}} = \mathbf{P}_1\left(\frac{b}{U}\right)^2 s^2 + \mathbf{P}_2\frac{b}{U}s + \mathbf{P}_3 + \mathbf{D}(s\mathbf{I} - \mathbf{R})^{-1}\mathbf{E}s \tag{20}$$

where $\mathbf{P}_i$, $\mathbf{D}$, and $\mathbf{E}$ are calculated from a least-square fit and $\mathbf{R}$ is a diagonal matrix. The diagonal terms of $\mathbf{R}$ are the aerodynamic poles and constants to be determined for the best fit of $\bar{\mathbf{Q}}$.

## III. Results and Discussion

Aeroelastic analyses were performed for a missile fin with an actuator (as shown in Fig. 1) in linear and nonlinear missile systems. The nonlinear missile system included a structural nonlinearity and dynamic stiffness in the actuator. The missile fin can be divided into upper and lower fins, and the upper fin can be folded to minimize a storage space. The upper fin was made of aluminum alloy, and the lower fin was made of steel. The missile fin was connected to the electric motor actuator.

### A. System Identification of the Actuator

Experimental tests and system identification of the actuator were needed to obtain the dynamic stiffness of the actuator for the aeroelastic analysis. Sine sweep tests of the missile fin actuator were performed according to several sweep ranges and applying forces. The experimental setup was arranged as shown in Fig. 3. Information

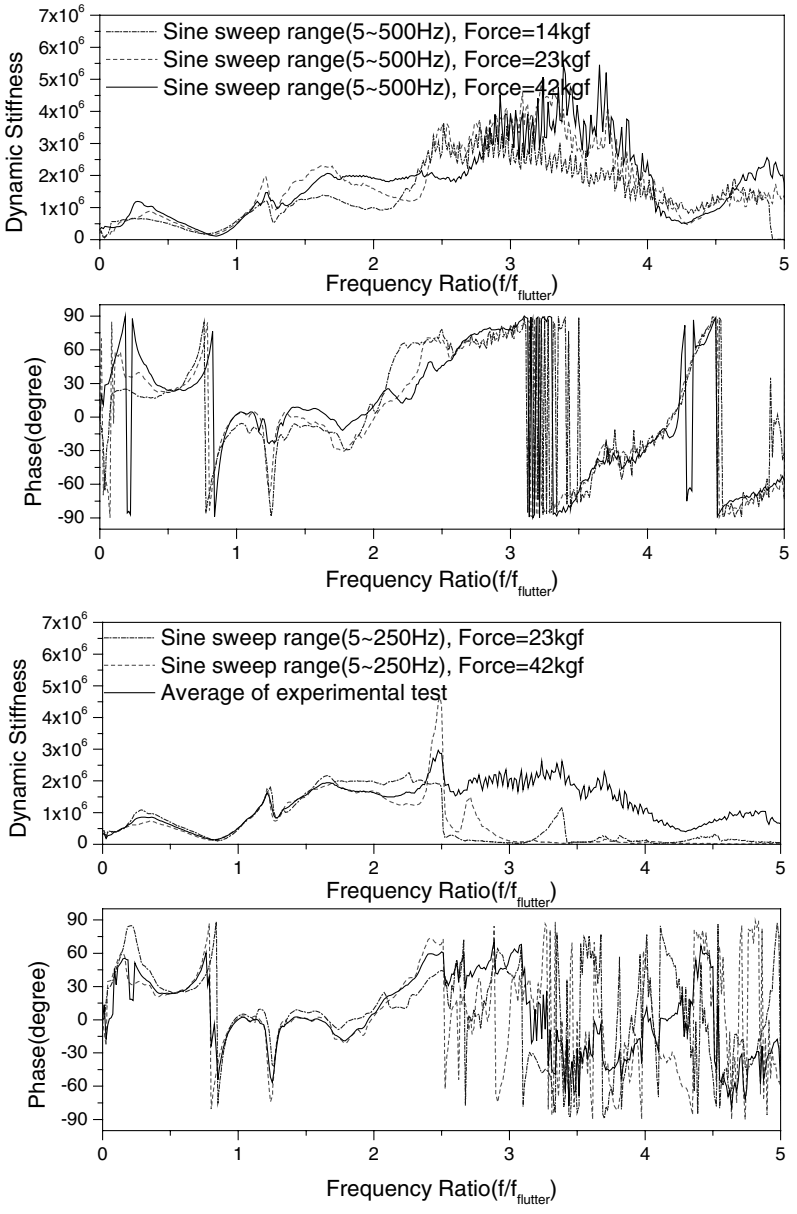


**Fig. 5 Dynamic stiffness of experimental tests of the missile fin system.**

**Table 2 Natural frequencies of the missile fin using the fictitious mass method**

| | $K_\theta = 4.9 \times 10^6$ N · mm/rad | | $K_\theta = 8.2 \times 10^6$ N · mm/rad | | $K_\theta = 1.4 \times 10^7$ N · mm/rad | |
|---|---|---|---|---|---|---|
| | FM | Direct | FM | Direct | FM | Direct |
| 1st mode, Hz | 48.12 | 48.12 | 48.18 | 48.18 | 48.22 | 48.22 |
| 2nd mode, Hz | 159.0 | 159.0 | 173.2 | 173.2 | 184.7 | 184.7 |
| 3rd mode, Hz | 304.6 | 304.6 | 307.0 | 307.0 | 308.5 | 308.5 |
| 4th mode, Hz | 392.7 | 392.7 | 393.4 | 393.4 | 394.1 | 394.1 |
| 5th mode, Hz | 624.0 | 624.0 | 624.5 | 624.5 | 624.9 | 624.9 |
| 6th mode, Hz | 683.7 | 683.7 | 683.8 | 683.8 | 683.8 | 683.8 |
| 7th mode, Hz | 904.9 | 904.9 | 904.9 | 904.9 | 906.0 | 906.0 |
| 8th mode, Hz | 11,635 | 953.4 | 13,664 | 953.5 | 16,871 | 953.6 |

on the applying forces and sweep ranges of the tests is listed in Table 1.

A shaker was used to oscillate the tip of the actuator load links, and a strain gage was applied to measure the angle displacement of the load links. The input data were the magnitudes of applying forces of the shaker, and these are controlled by computer. The output data were the angles of actuator load links, and they were obtained from the strain gage attached to the load links.

Figure 4 shows the power spectrum density between the input and output signals. The dynamic stiffness can be obtained from the relationship between the input and output power spectrum densities. Figure 5 shows the dynamic stiffness of each experimental test. The averaged results were applied for the aeroelastic analysis. The transfer function of the actuator is assumed as Eq. (10), and the parameters of the transfer function are calculated to fit the test results. The constrained optimization based Kuhn–Tucker equation is used to determine the parameters of the transfer function.

Several structural nonlinearities can exist in the actuator, such as transmission errors among the components of the actuator, the backlash of gears, the freeplay of load links, and the time delay of the electrical motor. In this actuator, no structural nonlinearity was found in the gears, but freeplay was found in the load links.

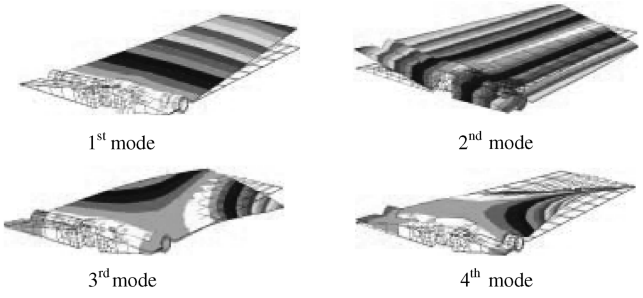


**Fig. 6 Natural mode shapes of the missile fin model ($K_\theta = 4.9 \times 10^6$ N · mm/rad).**

### B. Aeroelastic Characteristics

In the present study, the finite element method (FEM) was used for the free vibration analysis of the missile fin. Eight-node solid elements and bar elements were used to model the lower/upper fins and the hinge structures, respectively. Multipoint constraints were used to connect the lower/upper fins with the bar elements. A one-dimensional spring element for a root rotational spring was used, and point mass elements were used for the FM method. The root rotational spring indicated the boundary condition between the missile fin and the actuator. To improve computational time and efficiency, the FM method was often used in nonlinear flutter analysis. Validation of the FM method was performed, and Table 2 shows that the natural frequencies of the missile fin results using the FM method agreed with those of a direct model, except for the highest mode when the root rotational stiffness was changed. The direct model indicates that the boundary condition between the missile fin and the actuator is directly modeled with a root spring, whereas the FM model means that the boundary condition is represented with a fictitious mass instead of root spring. From the free vibration analysis, the FM model was established by adding a root spring. Figure 6 shows the lowest four modes of the missile fin. The first mode is the folding mode of an upper fin, and the second mode is the pitching mode. The third and fourth modes are the higher flexible modes of the upper fin. The disadvantage of the FM method is that the last mode among the structural modes, which are used for the FM method, does not match the original value. Thus, a sufficient number of structural modes were necessary to perform flutter analysis accurately.

The generalized mass and stiffness matrices and the mode shape of the free vibration analysis were used for the aeroelastic analyses. Mach number and air density used in the analyses were 0.7 and $1.23 \times 10^{-13}$ kgf · s$^2$/mm$^4$, respectively. In the present study, the iterative v-g method was used for a nonlinear aeroelastic analysis considering the structural nonlinearity and effects of the actuator.

The present aeroelastic analysis method was verified in previous studies [13]. The DHM code [14] was used to compute the subsonic unsteady aerodynamic forces, and a $10 \times 8$ mesh was used for the aerodynamic computation. This method was a combination of a

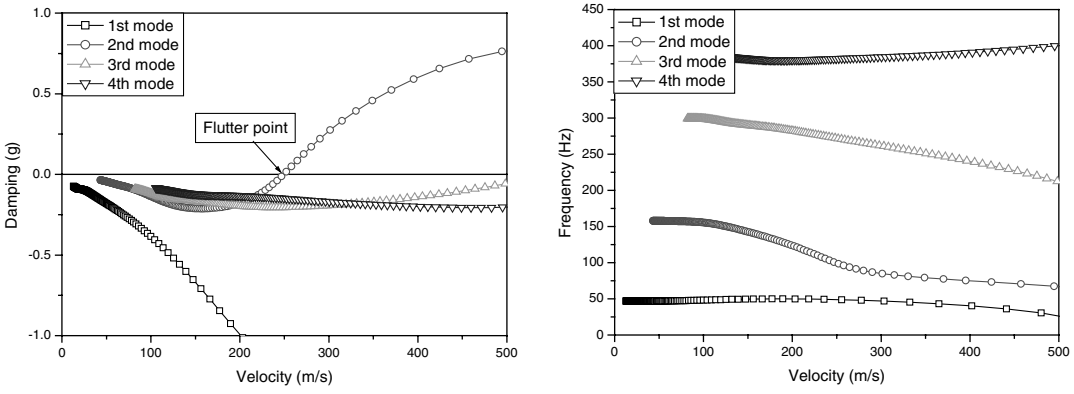


**Fig. 7 Linear flutter results of the missile fin model using the v-g method.**

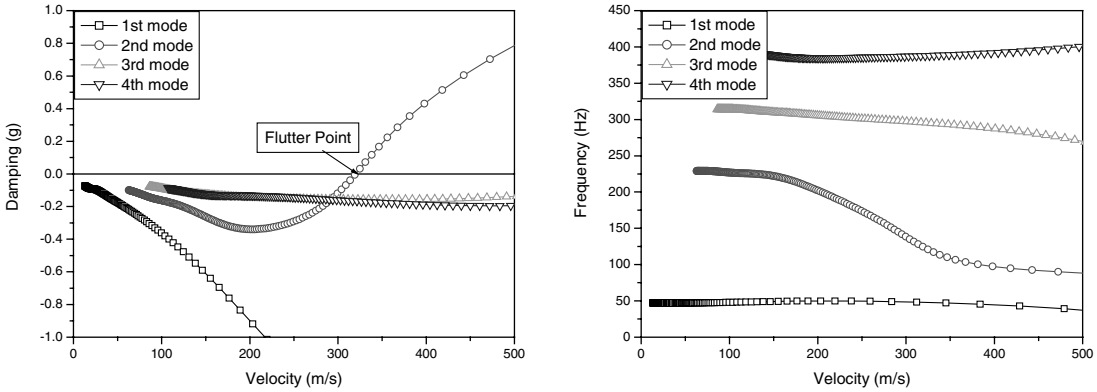


**Fig. 8 Flutter results of the missile fin model with dynamic stiffness using the iterative v-g method.**

doublet-point method (DPM) and a doublet-lattice method (DLM). The DPM is used to calculate the relation between the pressure difference at the doublet point and the downwash at the perceiving point using a kernel function. The DLM is used to compute the relationship between the pressure difference at the doublet line and the downwash.

A linear aeroelastic analysis without structural nonlinearity and dynamic stiffness for a missile fin was performed for a root rotational spring stiffness of 4.9 kN · m/rad. The linear flutter was obtained with the type of coalescence flutter between the folding and the pitch modes, as shown in Fig. 7. The first mode and the second mode frequencies approach each other when the velocity increases. Then, the two modes merged at the flutter point. In this model, the freeplay in the load links of the actuator affects the pitching mode that becomes the flutter mode. Hence, the change of the second mode frequency for a nonlinear case may affect the flutter boundary.

Then, to perform the flutter analysis in the frequency domain using the iterative v-g method, the iteration was repeated until converging one flutter point to 1%. Figure 8 shows the iterative v-g results of the missile fin with dynamic stiffness of the actuator. The flutter boundary, including the dynamic stiffness of the actuator, was improved by 28.35% in comparison with the linear flutter boundary. The dynamic stiffness was changed from 2 to 20 kN · m/rad in the flutter frequency regions as shown in Fig. 5.

To investigate the effects of variation of root stiffness on flutter boundary, linear aeroelastic analyses were performed for various root stiffnesses. Figure 9 shows that the linear flutter speed and frequency increase as the root stiffness increases. Flutter velocities and frequencies are normalized by the linear flutter velocity and frequency of Fig. 7, and root stiffness is also divided by 4.9 kN · m/rad. The improvements of the flutter boundary considering the dynamic stiffness are larger than those of the linear flutter boundary considering the variation of root stiffness. It seems

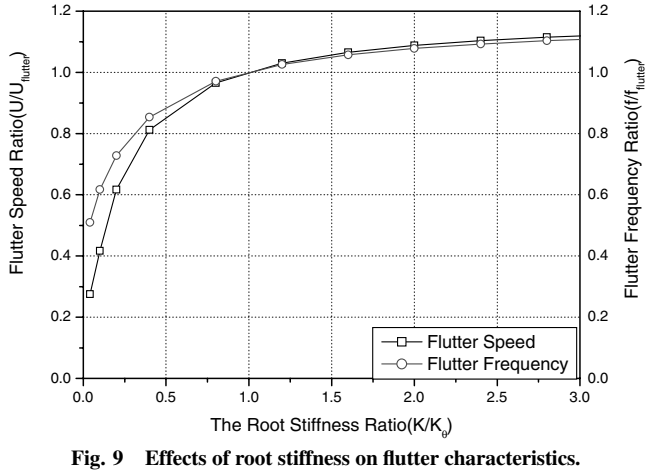


**Fig. 9 Effects of root stiffness on flutter characteristics.**

that not only the magnitude of dynamic stiffness but also the phase of the dynamic stiffness affects the flutter boundary.

Figure 10 shows the LCO characteristics of the missile fin with freeplay in the load links. The effects of dynamic stiffness were not considered, and the only nonlinearity of load links was considered. The results of frequency-domain analyses using the described function agreed with those of time-domain analyses. LCOs were observed above or below the linear flutter speed, because the flutter speed increases or decreases due to the variation of the equivalent stiffness.

However, LCO that occurs above the linear flutter boundary near the freeplay (when the nondimensional displacement, $\delta =$

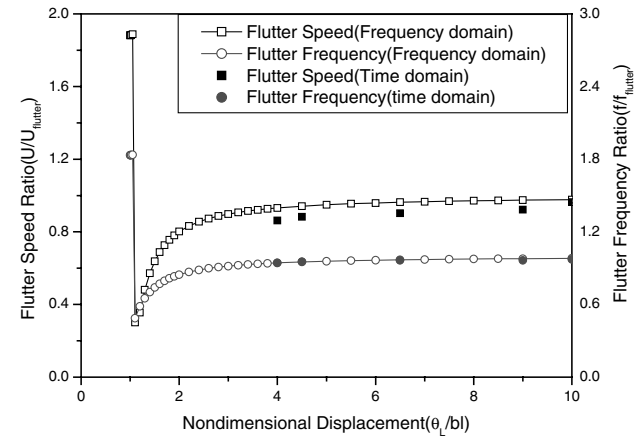


**a) Aeroelastic characteristics**

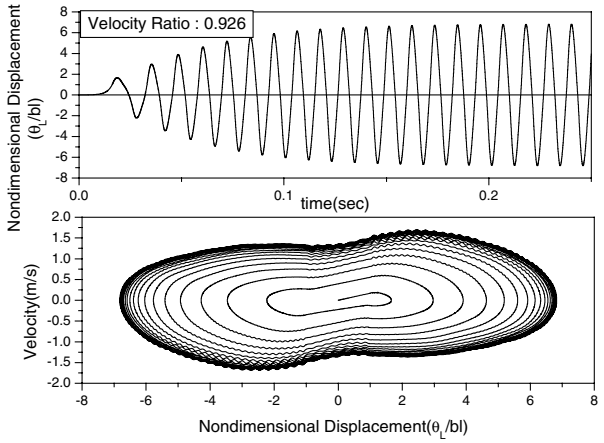


**b) Time response**

**Fig. 10 LCO characteristics of the missile fin with the freeplay in load links.**

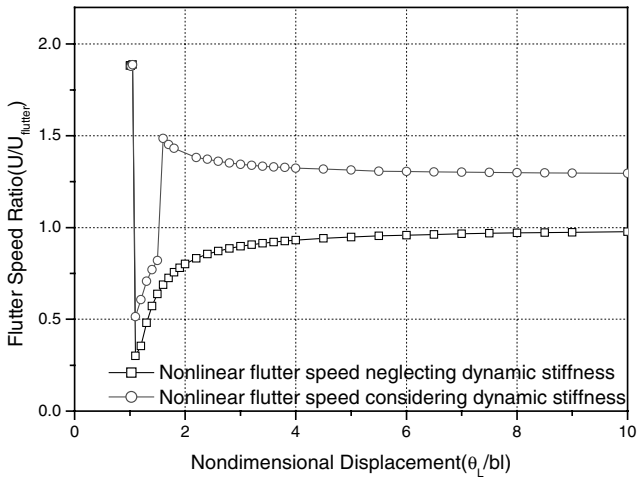


**a) Flutter speed**

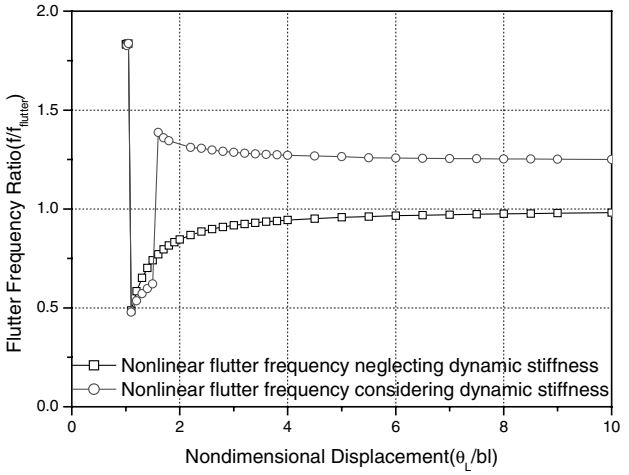


**b) Flutter frequency**

**Fig. 11 LCO characteristics of the missile fin with the freeplay in load links and the dynamic stiffness.**

$\theta_m/bl \approx 1$) is not meaningful, because the divergence speed is located below the flutter speed. In that case, divergence becomes main aeroelastic topics. The divergence boundary increases rapidly and is located above the flutter boundary as equivalence stiffness increases. Thus, the divergence does not make the system diverse to infinite, but the system maintains proper static deformation. When divergence speed occurs below flutter speed in a nonlinear system, biased LCO is often observed at the boundary of structural nonlinearity ($\delta \approx 1$). The LCO in Fig. 10b is a stable LCO for which flutter speed increases as the magnitude of oscillation increases. The nonlinear flutter boundary converges to a linear one as the magnitude of vibration increases.

The flutter frequency ratio shown in Fig. 10a is distributed from 0.5 to 1.0, except for the magnitude of the oscillation near $\delta \approx 1$. The variation of the dynamic stiffness is not negligibly small, as shown in Fig. 5. Figure 11 shows the LCO flutter characteristics of the missile fin with dynamic stiffness and the structural nonlinearity of the actuator using the iterative v-g method. The flutter boundary of the case considering the dynamic stiffness of actuator is higher than that of the case disregarding the dynamic stiffness for all nondimensional displacement. LCOs with only structural nonlinearity are observed below the linear flutter speed, except for near $\delta \approx 1$, but LCOs with structural nonlinearity as well as dynamic stiffness are located both above and below the linear flutter boundary.

The flutter boundary discontinuity is observed with $\delta = 1$–$1.5$ for the case with structural nonlinearity and dynamic stiffness. In addition, LCOs of two different types are observed. The flutter boundary improves as $\delta$ increases in these regions, but the flutter speed decreases as $\delta$ increases in the other regions. A stable LCO with a small amplitude and an unstable LCO with a large amplitude were observed. The flutter frequency ratio is distributed, from 0.5 to 0.8, with $\delta = 1$–$1.5$, and then discontinuity occurs after $\delta = 1.5$. It seems that the discontinuity of the flutter boundary is induced by the phase change of the dynamic stiffness. As shown in Fig. 5, the phase change of the dynamic stiffness is observed in those regions. These results show that the structural nonlinearity as well as the dynamic stiffness of the actuator may affect the flutter boundary significantly and that the flutter performance can change dramatically with a change of location of the poles or the zeros of the actuator. Hence, the effects of the poles and zeros of the actuator on the flutter characteristics should be seriously considered when designing the actuators for the missiles and aircrafts.

## IV. Conclusions

In this study, the nonlinear aeroelastic characteristics of a missile fin with an actuator have been investigated by using iterative v-g methods in subsonic regions, and the unsteady aerodynamic force coefficients have been calculated by using DHM based on a panel method. The dynamic stiffness of the actuator has been obtained by a sine sweep test, and the average value has been used for the aeroelastic analyses. LCOs were observed both below and above the linear flutter speed. The LCO characteristics of the aeroelastic system are significantly dependent on structural nonlinearity as well as dynamic stiffness. Thus, the structural nonlinearity and the dynamic stiffness play an important role in the nonlinear aeroelastic characteristics of an aeroelastic system. The aeroelastic boundary increases due to the effects of the actuator as compared with a case when only structural nonlinearity is considered. In addition, a discontinuity of the flutter boundary induced by the effects of the phase change occurs. The results also indicate that it is necessary to consider seriously the effects of the poles and the zeros of the actuator on the flutter characteristics to predict flutter behavior accurately when designing actuators of missiles or aircraft.

## Acknowledgment

The authors gratefully acknowledge the support of the Agency for Defense Development (ADD), Republic of Korea.

## References

[1] Woolston, D. S., Runyan, H. W., and Andrews, R. E., "An Investigation of Effects of Certain Type of Structural Nonlinearities on Wing and Control Surface Flutter," *Journal of Aeronautical Sciences*, Vol. 24, Jan. 1957, pp. 57–63.

[2] Laurenson, R. M., and Tron, R. M., "Flutter Analysis of Missile Control Surface Containing Structural Nonlinearities," *AIAA Journal*, Vol. 18, No. 10, 1980, pp. 1245–1251.

[3] Yehelzkely, E., and Karpel, M., "Nonlinear Flutter Analysis of Missiles with Pneumatic Fin Actuators," *Journal of Guidance, Control, and Dynamics*, Vol. 19, No. 3, 1996, pp. 664–670.

[4] McIntosh, S. C., Jr., Reed, R. E., Jr., and Rodden, W. P., "Experimental and Theoretical Study of Nonlinear Flutter," *Journal of Aircraft*, Vol. 18, No. 12, 1981, pp. 1057–1063.

[5] Yang, Z. C., and Zhao, L. C., "Analysis of Limit Cycle Flutter of an Airfoil in Incompressible Flow," *Journal of Sound and Vibration*, Vol. 123, No. 1, 1988, pp. 1–13.

[6] Lee, B. H. K., and Tron, A., "Effects of Structural Nonlinearities on Flutter Characteristics of the CF-18 Aircraft," *Journal of Aircraft*, Vol. 26, No. 8, 1989, pp. 781–787.

[7] Lee, I., and Kim, S. H., "Aeroelastic Analysis of a Flexile Control Surface with Structural Nonlinearity," *Journal of Aircraft*, Vol. 32, No. 4, 1995, pp. 868–874.

[8] Paek, S. K., and Lee, I., "Flutter Analysis for Control Surface of Launch Vehicle with Dynamic Stiffness," *Computers and Structures*, Vol. 60, No. 4, 1996, pp. 593–599.

[9] Conner, M. D., Tang, D. M., Dowell, E. H., and Virgin, L. N., "Nonlinear Behavior of a Typical Airfoil Section with Control Surface Freeplay: A Numerical and Experimental Study," *Journal of Fluid and Structures*, Vol. 11, No. 1, 1997, pp. 89–109.

[10] Liu, J. K., and Chan, H. C., "Limit Cycle Oscillations of a Wing Section with a Tip Mass," *Nonlinear Dynamics*, Vol. 23, No. 3, 2000, pp. 259–

270.
[11] Paek, S. H., Bae, J. S., and Lee, I., "Flutter Analysis of a Wraparound Fin Projectile Considering Rolling Motion," *Journal of Spacecraft and Rockets*, Vol. 39, No. 1, 2002, pp. 66–72.
[12] Librescu, L., Chiocchia, G., and Marzocca, P., "Implications of Cubic Physical/Aerodynamic Non-Linearities on the Character of the Flutter Instability Boundary," *International Journal of Non-Linear Mechanics*, Vol. 38, No. 2, 2003, pp. 173–199.
[13] Bae, J. S., Kim, D. K., Shin, W. H., Lee, I., and Kim, S. H., "Nonlinear Aeroelastic Analysis of a Deployable Missile Control Fin," *Journal of Spacecraft and Rockets*, Vol. 41, No. 2, 2004, pp. 264–271.
[14] Ueda, T., and Dowell, E. H., "A New Solution Method for Lifting Surfaces in Subsonic Flow," *AIAA Journal*, Vol. 20, No. 3, 1982, pp. 348–355.
[15] Karpel, M., "Design for Active Flutter Suppression and Gust Alleviation Using State-space Aeroelastic Modeling," *Journal of Aircraft*, Vol. 19, No. 3, 1982, pp. 221–227.
[16] Press, W. H., Flanner, B. P., Teukolsky, S. A., and Vetterling, W. T., *Numerical Recipes: The Art of Scientific Computation*, Cambridge University Press, Cambridge, U.K., 1986.
[17] Gelb, A., and Vander Velde, W. E., *Multiple-Input Describing Functions and Nonlinear System Design*, McGraw–Hill, New York, 1986.
[18] Karpel, M., and Newman, M., "Accelerated Convergence for Vibration Modes Using the Substructure Coupling Method and Fictitious Coupling Masses," *Israel Journal of Technology*, Vol. 13, Feb. 1975, pp. 55–62.